
Inverse Problems Leveraging Pre-trained Contrastive Representations

Sriram Ravula*

The University of Texas at Austin
Electrical and Computer Engineering
sriram.ravula@utexas.edu

Georgios Smyrnis*

The University of Texas at Austin
Electrical and Computer Engineering
gsmyrnis@utexas.edu

Matt Jordan

The University of Texas at Austin
Computer Science
mjordan@cs.utexas.edu

Alexandros G. Dimakis

The University of Texas at Austin
Electrical and Computer Engineering
dimakis@austin.utexas.edu

Abstract

We study a new family of inverse problems for recovering representations of corrupted data. We assume access to a pre-trained representation learning network $R(x)$ that operates on clean images, like CLIP. The problem is to recover the representation of an image $R(x)$, if we are only given a corrupted version $A(x)$, for some known forward operator A . We propose a supervised inversion method that uses a contrastive objective to obtain excellent representations for highly corrupted images. Using a linear probe on our robust representations, we achieve a higher accuracy than end-to-end supervised baselines when classifying images with various types of distortions, including blurring, additive noise, and random pixel masking. We evaluate on a subset of ImageNet and observe that our method is robust to varying levels of distortion. Our method outperforms end-to-end baselines even with a fraction of the labeled data in a wide range of forward operators.

1 Introduction

Modern representation learning networks like CLIP [35] are showing incredible performance for image classification, even for zero-shot problems with labels not seen during training. Training these encoders comes at a staggering cost and requires datasets and computing resources only available to very few organizations. In this paper we show how to leverage this pretrained power for a new family of problems in the presence of image corruptions or other types of measurements.

Inverse problems involve reconstructing an unknown vector x from measurements $y = A(x)$. Typically, the forward operator A corrupts the unknown vector x and reduces its dimension, i.e. the observations y live in a lower-dimensional space compared to x . In the special case of linear inverse problems, the forward operator is simply a matrix and the measurements are in the form $y = Ax + \text{noise}$. Special cases of linear inverse problems include image denoising, inpainting, super-resolution, compressed sensing used in medical tomography, seismic geological imaging and many others, see e.g. [31] for a recent overview.

*Equal contribution.

Code available at <https://github.com/Sriram-Ravula/Contrastive-Inversion>.

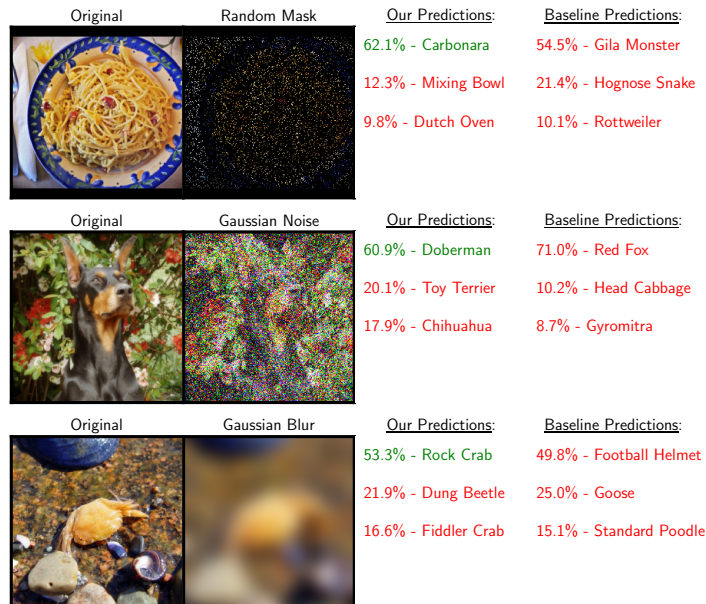


Figure 1: **Predictions of our models vs. supervised baselines for corrupted images.** Our robust encoders observe highly corrupted images and use a simple linear probe to classify in ImageNet-100 labels. We present the top 3 classes from our models as well as those from the end-to-end supervised baselines trained with the same amount of labeled data, for select images. For three different types of forward operators (90 percent missing pixels, strong Gaussian noise and high Blurring) our robust encoders classify correctly and also produce reasonable top 3 alternatives. On the contrary, the supervised baselines completely fail even though they were fine-tuned on exactly this task to classify corrupted images, starting from a powerful ImageNet pretrained ResNet-101. We also expect that most humans would fail to classify such highly corrupted images – more examples are included in the Appendix.

In this paper we introduce the study of a new family of inverse problems: reconstructing the representation of an image given a corrupted or measured input. Formally, if a (clean) image is x and its CLIP representation is $R(x)$, we would like to obtain that representation by only observing a highly corrupted input $A(x)$. This is impossible if the forward process A removes information needed to obtain the representation. Surprisingly, we show that it can be very well approximated even from extremely corrupted versions of the image.

We introduce a robust encoder S that is trained to imitate the behavior of the pretrained CLIP encoder acting on clean images x . However, the input to the robust encoder is only corrupted images $A(x)$ that are created by applying the forward operator on x . Our approach is illustrated in Figure 2. The teacher encoder is the pretrained CLIP, and the student encoder is our robust encoder operating on corrupted images. Formally, the robust encoder $S(A(x))$ is trained to approximate $R(x)$ using a contrastive loss.

1.1 Results

We show that our method is able to obtain useful representations even under extreme corruptions such as removing 90% of the pixels as shown in the top panel of Figure 1. The highly corrupted images enter our robust encoder and the obtained representation is used in a linear classifier to produce ImageNet-100 labels. Our main result is that our method outperforms a pretrained ResNet (of the same size as our robust encoder) fine-tuned end-to-end on labeled distorted images.

Using less labeled data For some corruption levels, we are able to outperform end-to-end fine-tuned ResNets using as little as 10% of labeled samples. This is even when the fine-tuned baseline uses 100% of ImageNet-100 labels for training. The primary advantage of our model is that our robust encoder observes representations from the pretrained CLIP encoder, which was trained with a much bigger dataset compared to ImageNet. Still, the fact that this implicit advantage in the representations and 10% of labeled data is sufficient to outperform a supervised trained ResNet fine-tuned with 10

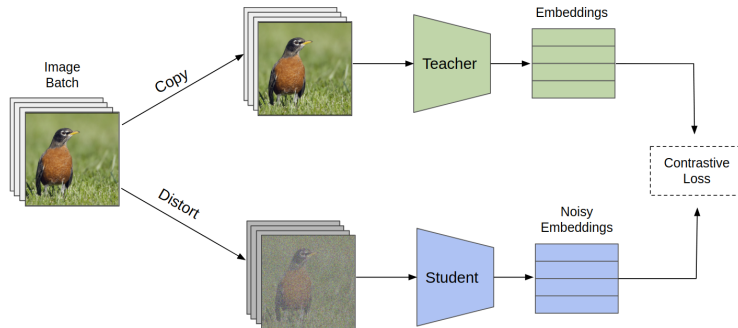


Figure 2: **Overview of our proposed method.** We initialize a student and teacher model from a pretrained CLIP encoder. Clean image batches are fed to the teacher while distorted versions of those images are fed to the student. The student is trained using a contrastive loss which makes student and teacher representations of the same original images more similar while making their representations of different images less similar.

times more labeled data is very surprising and illustrates the power and versatility of pretrained representation learners.

Robustness to noise and data shifts Our method is very robust to changes in the forward operators, data statistics and label shifts. We experiment with three classes of forward operators: random pixel masking, additive Gaussian noise, and Gaussian blurring distortions. For each, we train and test on a wide-range of distortion levels, from slight to severe corruption. We show that our robust encoder produces useful representations even when the level of corruption is outside its training domain.

We show that our representations are useful for a wide range of tasks, without requiring knowledge of the task when the robust encoder is trained. We illustrate excellent classification accuracy across five datasets, frequently outperforming end-to-end supervised baselines trained with knowledge of the target task. Our experiments include a chest X-ray COVID pneumonia task which has very different morphology compared to ImageNet. Surprisingly, the same universal representations, combined with a custom linear probe are very successful across all tasks.

Contrastive versus MSE training We formulate the contrastive student training method as a regularization upon the simple mean squared error loss between student embeddings of a distorted image and teacher embeddings of the clean version of that image. We analyze the effects of this regularization on the training dynamics. Our results empirically show that the latter lags behind in most cases in performance, further strengthening our argument for the usefulness of contrastive learning in this setting.

2 Related Work

Robust Image Recognition It has been shown that classifiers that perform well on clean image tasks are not robust to common image distortions [21]. Several datasets have been proposed specifically to benchmark generalization of classifier performance to natural distortions [18, 38]. Related to our work, [45] and [12] fine-tune pretrained classifiers on distorted data, which seems to yield better performance than end-to-end training. However even under these training processes, modern classifiers exhibit inferior performance to human vision on distorted data [12].

Inverse problems There is significant recent literature on solving inverse problems including denoising, inpainting and deconvolution for deblurring. While classical techniques rely on sparsity based priors e.g. [30, 37], recent techniques include data-driven deep-learning methods [1, 10, 13, 33] as well as combinations of sparsity and generative methods [11] and untrained deep nets [16]. Our work focuses on recovering the representation of an image, as opposed to an image itself, so it is also related to task-aware sensing [23]. However, our approach is fundamentally different from all previous inverse problems since it leverages a pretrained representation network teacher (namely CLIP). In the Appendix, we compare to methods that attempt to solve the inverse problem in pixel space and then apply a classifier on the inpainted and denoised image. The other important distinction is that even though our corruption processes are linear in the pixel space, they are non-linear with

respect to the representation vector we try to recover. In effect, we are solving a non-linear inverse problem in a supervised way using a contrastive loss.

Contrastive Representation Learning Self-supervised representation learning has recently exploded in popularity, largely due to the success of contrastive losses in learning representations from unlabeled data [4, 6, 7, 15, 17, 43]. These techniques are able to generate highly general embeddings of images that are effective for many types of downstream tasks, even on domains that were not explicitly considered in training [27]. Contrastive losses generally operate based on a simple push-pull principle: images desired to be close in embedding space are pushed together, while unrelated images are pulled apart. One particularly popular choice of contrastive loss is the InfoNCE loss, derived from techniques for noise contrastive estimation [14], and popularized in the self-supervised setting in [32]. Several works have considered adversarial training frameworks to yield representations that are more robust to adversarial attacks [20, 22, 25]. However these works only consider adversarial robustness and not robustness to common corruptions. Our approach is similar to that of [24], which employs a variant of the InfoNCE loss for a supervised setting. This differs from our work in that we exclusively focus on robustness to natural corruptions and propose a fundamentally unsupervised approach where we have no knowledge of labels when learning the representations.

Knowledge Transfer Methods Our work is closely related to prior works which aim to distill, reduce, or transfer the knowledge from one network to another for a specific task [3, 19, 29, 44]. Of note is [40], where the authors use a contrastive objective to transfer representations from a teacher network to a student network. Our work diverges in that we do not transfer from a larger, more powerful teacher to a smaller student, but rather transfer between a teacher and student of the same architecture initialized from the same weights. In addition, although the authors test on cross-modal transfer tasks such as transferring between color channels, transferring representations between clean and distorted images is a different task: we try to extract the same high-level information from *less data* as opposed to *different, but related data*.

3 Method

Our problem is to recover the embeddings of clean images when we only have access to highly corrupted versions of the images. The *encoder* $R(\cdot)$ is assumed to yield high-quality representations for a variety of domains. The *distortion process* $A(\cdot)$ is assumed to be a known forward operator that greatly distorts images. We assume $A(\cdot)$ is sufficiently severe as to inhibit the performance of the encoder $R(\cdot)$, but not so severe that recovery is impossible. From a collection of input images $\{x_i\}_{i=1}^N$, we are only given access to the distorted images and the representations of the clean images $\{A(x_i), R(x_i)\}_{i=1}^N$. Our approach is to learn a student function S so that $S(A(\cdot))$ is equally useful as the teacher representation $R(\cdot)$. We measure the utility of a representation by the performance on an unspecified downstream supervised learning task.

Least squares Loss One potential approach for the task of recovering the teacher’s embeddings from the corrupted inputs is to minimize the expected ℓ_2 distance in embedding space between the clean teacher embeddings $R(\cdot)$ and the predicted student representations $S(A(\cdot))$. If both $R(\cdot)$ and $S(\cdot)$ are constrained to have ℓ_2 -normalized outputs, then the empirical least squares loss becomes:

$$\hat{\mathcal{L}}^{\text{MSE}}(S; R, A) := \frac{-1}{N} \sum_{i=1}^N \langle S(A(x_i)), R(x_i) \rangle, \quad (1)$$

where we have expanded and subtracted out constant terms. However, this process may not yield the most effective embedding of the corrupted data. Due to either limitations in the training process, the severity of the distortion process, or the generalization properties of the approximate minimizers of $\hat{\mathcal{L}}^{\text{MSE}}$, the learned embeddings $S(A(\cdot))$ may not be as useful for downstream tasks as embeddings learned using the other losses we consider.

Contrastive Loss Inspired by recent advances in self-supervised representation learning, we learn S by minimizing a contrastive loss. We consider the following variant on the popular InfoNCE loss:

$$\hat{\mathcal{L}}^{\text{contr}}(S; \tau, R, A) := \frac{-1}{N} \sum_{i=1}^N \log \frac{\exp(K(i, i)/\tau)}{\sum_{j=1}^N \exp(K(i, j)/\tau)}, \quad (2)$$

where $K(i, j) := \langle S(A(x_i)), R(x_j) \rangle$ measures the similarity between the learned embedding of $A(x_i)$ and the clean embedding of x_j , and τ is a temperature hyperparameter. We follow [5, 42] and rewrite $\hat{\mathcal{L}}^{\text{contr}}$ in terms of explicit ‘pull’ and ‘push’ terms as :

$$\hat{\mathcal{L}}^{\text{contr}}(S; \tau, R, A) = \frac{1}{\tau} \hat{\mathcal{L}}^{\text{MSE}}(S; R, A) + \hat{\mathcal{L}}^{\text{unif}}(S; \tau, R, A), \quad (3)$$

where the second term, referred to as the uniformity term, is defined as:

$$\hat{\mathcal{L}}^{\text{unif}}(S; \tau, R, A) := \frac{1}{N} \sum_{i=1}^N \log \sum_{j=1}^N e^{K(i,j)/\tau}. \quad (4)$$

The first term of $\hat{\mathcal{L}}^{\text{contr}}$ is simply $\hat{\mathcal{L}}^{\text{MSE}}$ which encourages alignment of $S(A(x_i))$ with $R(x_i)$, and the $\hat{\mathcal{L}}^{\text{unif}}$ term encourages the learned representations for corrupted data to be dissimilar from all other representations of clean data.

The primary difference between Equation 3 and the InfoNCE loss commonly used in self-supervised learning is the choice of the similarity measure $K(\cdot, \cdot)$. Without access to specified target embeddings, $K(i, j)$ is typically chosen to be the inner product between projections of the embeddings of x_i and x_j , (or between x_i and a positive example in the case of $K(i, i)$). Here, the uniformity term is necessary to prevent representation collapse, where in our setting $\hat{\mathcal{L}}^{\text{MSE}}$ alone suffices to prevent this degenerate case. We note that alternative choices for $K(\cdot, \cdot)$ in $\hat{\mathcal{L}}^{\text{unif}}$ may be employed. For example, we could also contrast the student embeddings $S(A(\cdot))$ across two different images. We ablate against other choices in the experimental section and find that our choice of $K(\cdot, \cdot)$ is one of several that exhibits comparable performance.

Effect of uniformity term To examine the effect of the uniformity term of the loss on the training dynamics, we consider the gradients of $\hat{\mathcal{L}}^{\text{contr}}$ with respect to the parameters of the encoder S . We first decompose $\hat{\mathcal{L}}^{\text{unif}}$ to consider the contributions of each individual data point:

$$\hat{\mathcal{L}}^{\text{unif}}(S; \tau, R, A) = \frac{1}{N} \sum_{i=1}^N \hat{\mathcal{L}}_i^{\text{unif}}(S; \tau, R, A), \quad \hat{\mathcal{L}}_i^{\text{unif}}(S; \tau, R, A) := \log \sum_{j=1}^N e^{\frac{K(i,j)}{\tau}}.$$

Then the gradient of $\hat{\mathcal{L}}^{\text{contr}}$ with respect to the parameters of S may be written as

$$\nabla_S \hat{\mathcal{L}}^{\text{contr}}(S; \tau, R, A) = \frac{-1}{\tau} \nabla_S \hat{\mathcal{L}}^{\text{MSE}}(S; R, A) + \frac{1}{\tau N} \sum_{i=1}^N \sum_{j=1}^N w_i(j) \nabla_S K(i, j),$$

where

$$w_i(j) := \exp \left(K(i, j)/\tau - \hat{\mathcal{L}}_i^{\text{unif}}(S; T, R, A) \right).$$

This can be interpreted as follows. The weighting of the first term by τ^{-1} balances the gradients $\nabla_S K(i, i)$ and $\sum_j \nabla_S K(i, j)$, as is common with other choices of contrastive losses (c.f. Theorem 2 in [41]). Noting that for each i , the weights $w_i(j)$ sum to 1, the gradient of each individual uniformity term $\hat{\mathcal{L}}_i^{\text{unif}}$ is a convex combination of the gradients of the similarity terms $K(i, \cdot)$. The individual similarity terms are weighted exponentially proportionally to each $K(i, j)$ ’s contribution to the total uniformity loss. As τ decreases, the weights place greater emphasis on terms that are most similar. As τ is commonly chosen to be less than 1, the dynamics automatically reflect the influence of the ‘hardest’ negative examples.

When is perfect recovery possible? Finally, we describe conditions which allow for perfect recovery of the clean embeddings from the corrupted images in the training set. The first condition is that the corruption process should not be too destructive: it suffices to assume that the implication $A(x_i) = A(x_j) \implies R(x_i) = R(x_j)$ holds for all x_i, x_j in the training set, i.e., there exists a function which attains exact recovery. In this case, any S^* that minimizes $\hat{\mathcal{L}}^{\text{MSE}}$ has $S^*(A(x_i)) = R(x_i)$ for all x_i in the training set. To argue for the same recovery guarantees when optimizing $\hat{\mathcal{L}}^{\text{contr}}$, we need to assume that the teacher $R(\cdot)$ provides a well-separated embedding of the training data.

Proposition 1. *If R is a minimizer of the uniformity term*

$$R \in \arg \min_f \sum_{i=1}^N \log \sum_{j=1}^N \exp \frac{\langle f(x_i), f(x_j) \rangle}{\tau},$$

then any encoder $S^ \in \arg \min_S \hat{\mathcal{L}}^{\text{contr}}(S; \tau, R, A)$ exactly recovers the target embedding, $S^*(A(x_i)) = R(x_i)$ for all x_i in the training set.*

4 Experiments

We show that the proposed training process recovers useful representations from corrupted inputs for a variety of forward operators, evaluating several different classification tasks. We start by evaluating the representation quality when the distortion process and data distribution are the same during both training and inference, examining the label-efficiency of our approach.

Then we evaluate our approach when the severity of the distortions changes at test time, when the test data distribution differs from the one used during training, and when the labels are shifted. Finally, we ablate against alternative formulations of our loss function.

For all experiments, we pretrain the robust encoder using a 100-class subset of ImageNet, which we refer to as ImageNet-100, [36, 39] to reduce computational resources. Our target representations are attained from the CLIP ResNet-101. We fine-tune with our training process and evaluate by training a linear classifier on top of the frozen representations. Our baselines are built on a ResNet-101 initialized with weights from supervised training on the full ImageNet dataset. The final fully-connected layer is replaced with a 100-dimensional output. We fine-tune the whole model in a supervised fashion using distorted inputs and their correct labels from ImageNet-100. The baseline is trained for 25 epochs with a batch size of 64. Our robust encoder is trained for 25 epochs with a batch size of 256, and the linear probe on top of it is trained for 10 epochs. Further details on training and hyperparameter choices are discussed in the appendix and in our provided code.

4.1 Known Data Distribution and Forward Operator

In this section, we evaluate the quality of the learned robust representations for classifying images from the validation set of ImageNet-100, using the same distortions during training and inference. These experiments demonstrate the usefulness of our method for vision inverse problems where the data distribution and forward operator are both known at training time. We also demonstrate the label-efficiency of our approach by evaluating our learned representation when only few labeled samples are available to train the linear classifier.

Setup We train the robust contrastive model and the baseline as described above. Eight different distortion processes are examined: Gaussian blur with (kernel size, standard deviation) of (21, 5) and (37, 9); additive Gaussian noise with standard deviations 0.1, 0.3, and 0.5; and random pixel mask with 50%, 75%, and 90% of the pixels missing. We evaluate our method against the baseline in top-1 accuracy on the validation set of ImageNet-100, under the same distortion used to train each model. To demonstrate the label-efficiency of our method, we also train a linear probe with only 10% of the labeled data, and for two of our models we train linear probes using various amounts of labeled data.

Results In Table 1, we see that training a linear probe on top of the representations learned by our procedure greatly improves accuracy compared to the supervised baseline. This further solidifies our original motivation. Furthermore, we can see that using only 10% of labeled samples is sufficient for our model to outperform the baseline in most cases. More fine-grained label-efficiency results can be seen in Figure 3, where we show that in two of these cases, using just 5% of the labeled data makes our model outperform or be competitive with the baseline trained using all the labels.

4.2 Known Data Distribution and Unknown Forward Operator

In many settings, the data distribution and the *type* of distortion will be known at training time, but the *severity* of the distortion will be unknown. We consider the case where the severity of the distortion at test-time is greater than what was seen during training.

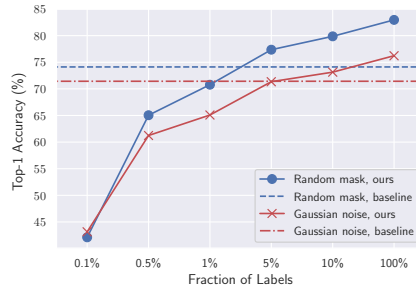


Figure 3: **Accuracies using a varying fraction of labeled samples to train a linear probe.** We train robust encoders on images with 90% random pixel masking and additive Gaussian noise with standard deviation 0.5, and fit a linear classifier on the learned representations using varying fractions of labeled training samples. We compare to a supervised baseline that uses all of the labeled training samples. Results are averaged over 10 random instantiations of corruptions on the ImageNet-100 validation dataset. We omit error bars as standard error is insignificant.

Table 1: **Top-1 accuracy (percent) on ImageNet-100.** The best accuracy for each distortion is bolded. Each model is trained using images with a fixed type of distortion. We train our robust CLIP encoder contrastively, then fit a linear probe on the learned representations using either all or 10% of the labeled training samples. We report the mean and standard error for accuracy over 10 random instantiations of distortions on the ImageNet-100 validation dataset (Gaussian blur is deterministic, so we do not include standard error values). For Gaussian blur, n corresponds to the length of the blur kernel.

Distortion	Supervised Baseline	Ours	Ours (10% labeled data)
Random Mask 50%	77.53±0.06	85.87±0.08	82.19±0.08
Random Mask 75%	75.68±0.06	83.99±0.07	80.36±0.09
Random Mask 90%	74.12±0.09	82.96±0.08	79.87±0.12
Gaussian Noise $\sigma = 0.1$	82.23±0.04	84.46±0.08	80.99±0.09
Gaussian Noise $\sigma = 0.3$	75.78±0.08	81.30±0.07	78.16±0.07
Gaussian Noise $\sigma = 0.5$	71.43±0.14	76.23±0.10	73.14±0.08
Gaussian Blur $n = 21$	76.40	83.24	80.94
Gaussian Blur $n = 37$	68.94	77.80	74.84

Setup First, we train a model using training images with between 50 and 95% of pixels randomly masked. In addition, we train a model using images with additive Gaussian noise with random standard deviation between 0.1 and 0.3. Once fully trained, we fit a linear classifier on top of the learned representations for each model using the same distortions. We also train two supervised baselines end-to-end with the same distortions. We evaluate the models trained with pixel masking on images with a fixed level of 96 to 99% percent missing pixels, and the networks trained with noise on images with additive Gaussian noise using a fixed standard deviation between 0.35 and 0.5.

Results In Figure 4, we see that with an increase in noise levels, the accuracy of the models does decrease. However, the linear probe trained on the entire dataset achieves better results than the baseline end-to-end supervised model. This shows that our model is more robust, even when the distortions are greater than those expected during training.

4.3 Unknown Data Distribution and Known Forward Operator

In this section we evaluate how well ImageNet pretraining with distortions allows the learned representations to transfer to different datasets. We use the same forward operator during training and inference to isolate the quality of the embeddings learned by contrastive pretraining even in the presence of distortion.

Setup Five datasets are chosen to evaluate transferability of robust representations. (1) CIFAR-10 and (2) CIFAR-100 [28], and (3) STL-10 [8]. (4) The COVID-19 Chest X-ray dataset [9], (5) We generate another random 100-class subset of ImageNet [36] from the remaining 900 classes we did not use for ImageNet-100, which we refer to as ImageNet-100B.

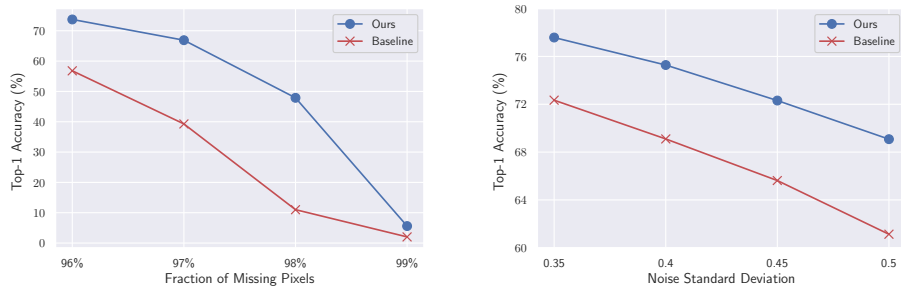


Figure 4: **Accuracies for images with varying corruption levels using models trained on a range of levels.** In the left figure, we compare our robust model with a baseline, both trained on images with 50% to 95% random pixel masking. In the right figure, each model is trained on images with additive Gaussian noise with random standard deviation from 0.1 to 0.3. We evaluate the models on images with more severe corruptions than applied during training. Results are averaged over 10 random instantiations of corruptions on the ImageNet-100 validation dataset. We omit error bars as standard error is insignificant.

Table 2: **Top-1 accuracies for transfer learning.** We fit a linear classifier for each dataset on top of the representations learned by the models from ImageNet-100. RM means the model was trained with random missing pixels, and GN means it was trained with additive Gaussian noise. Results are mean and standard errors over 10 realizations of the distortions during evaluation.

Model	CIFAR-10	CIFAR-100	STL-10	COVID X-ray	ImageNet-100B
Baseline (RM)	79.83±0.04	55.10±0.08	81.09±0.05	82.07±0.23	67.45±0.09
Ours (RM)	80.93±0.04	58.55±0.09	89.44±0.05	84.01±0.20	80.09±0.07
Baseline (GN)	76.52±0.07	52.00±0.05	82.28±0.07	83.54±0.15	69.49±0.11
Ours (GN)	76.19±0.09	52.51±0.09	86.30±0.08	79.74±0.26	78.66±0.13

We train the same models under the same distortions as outlined in Section 4.2, then fit linear classifiers for the new datasets on top of the fixed representations. Preprocessing details for each dataset may be found in the Appendix. We calculate top-1 accuracy of each model for classifying distorted images from the validation or test set of each of the new datasets. The images are distorted using the same forward operators used to train the networks.

Results Table 2 shows that our approach can achieve good results in a variety of datasets. In CIFAR-10 and CIFAR-100, we get results comparable to the baseline. In STL-10, we have greater top 1 accuracy for both noise settings. For the COVID X-ray dataset, we get mixed results, where we beat the baseline for the random masking model, but we lose for the additive Gaussian noise model. The most surprising result is the vast increase in accuracy for the alternative ImageNet-100B dataset. This shows that due to the supervised training of the baseline, some information from the labels leaks into the representation, leading to worse performance on a related, but ultimately different dataset.

4.4 Label Shift

An important factor in determining the robustness of a model is how gracefully it fails in the presence of unseen data modalities at inference time. For instance, if a network trained to distinguish dogs from cars is shown an image of a cat, the network should produce an embedding which is more likely to be classified as a dog than a car. This is even more important for inverse problems: a single distorted image may result from the same forward operator being applied to any number of original images. If a distorted image from a class outside of the training classes makes a network output an unexpected or uninformative representation, then the network is likely also brittle to shifts in the data distribution *within the classes it knows* at inference time. We evaluate the quality of representations produced by our method for distorted images from classes outside of the training dataset.

Setup We use the same models described in Section 4.2. To simulate images from unseen classes, we identify 5 classes from the validation set of full ImageNet that were not used in our training data,

Table 3: **Label Shift: Out of Distribution ImageNet Classes and their New Labels.** We list the five ImageNet classes taken from outside of ImageNet-100 and the new labels given to them based on similar classes from within ImageNet-100.

ImageNet Class	New ImageNet-100 Label
Cup	Cocktail Shaker
Dungeness Crab	Rock Crab
Mountain Bike	Moped
Wood Rabbit	Hare
French Bulldog	American Staffordshire Terrier

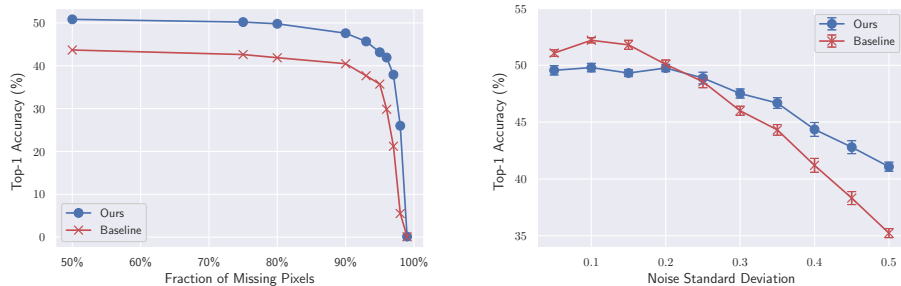


Figure 5: **Accuracies for varying noise levels on unseen classes using label shift.** On the left, we see the model trained on 50% to 95% random masking of pixels, while on the right the model trained on Gaussian noise with standard deviation from 0.1 to 0.3. Both models are evaluated on the unseen classes, using the chosen reference classes from ImageNet100 as the targets, as shown in the label shift table. Results are averaged over 10 random instantiations of corruptions. We omit error bars in the left figure as standard error is insignificant.

but are similar to classes within our training data. We replace the labels of these new images with the label of the classes in our training data that are similar to them, as seen in Table 3. Evaluation is done on images from these replacement classes, under fixed levels of distortion, with 50% to 99% missing pixels on the random masking model and 0.05 to 0.5 standard deviation for the Gaussian noise model.

Results In Figure 5, we can see that, for the random pixel mask case, we consistently outperform the baseline across all noise levels. For the Gaussian noise case, our model has slightly lower top-1 accuracy for small noises. This can be explained by the fact that small distortions do not drastically alter the image, so the baseline is bolstered by its ImageNet pretraining. However, as the noise level increases, the baseline model degrades much more quickly.

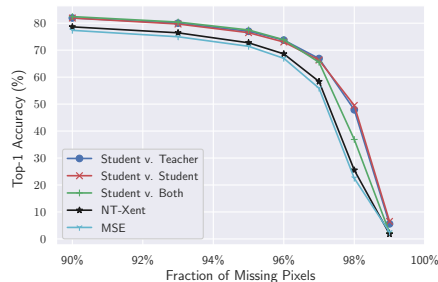


Figure 6: **Ablation study.** We evaluate the model trained on 50% to 95% random masking of pixels, using several variants of the uniformity term in the contrastive loss. Results are averaged over 10 random instantiations of corruptions on the ImageNet-100 validation dataset. We omit error bars as standard error is insignificant.

4.5 Ablation: Training Loss

Finally, we ablate against various choices for the uniformity term in the contrastive loss. We consider variants of $\hat{\mathcal{L}}^{\text{unif}}$ where we compare representations of i) the student and teacher, ii) the student and the student, iii) a sum of both of the above. We also consider $\hat{\mathcal{L}}^{\text{MSE}}$, i.e. no uniformity term, as well as one variant where every representation is contrasted with every other representation (irrespective of student or teacher), which we note is the same formulation as NT-Xent as used in SimCLR [6].

Setup We use the same random masking model described in Section 4.2, with a similar evaluation on fixed masking levels of 90-99%. Explicit formulations of each of the losses is in the appendix.

Results We draw two main conclusions from Figure 6. First, the MSE loss performs worst, indicating the benefit of the uniformity term in the loss. Next we see that all student comparisons perform roughly equivalently, but are clearly more effective than MSE and NT-Xent.

5 Conclusion

In this work, we propose a method for training image representation networks which are robust to various distortions on the input data. This has potential for improving the practical applications of neural networks. Indeed, images in real-world settings are rarely exemplary: every stage of the imaging process, from capture to storage to transmission and display, can introduce noise or distortions in the images. Mitigating this sensitivity to distortions will enable more applications to harness the power of deep learning models. Moreover, this process helps reduce the cost of training such models, both with respect to computation (since we can add robustness to a pre-trained model, instead of training one from scratch), as well as with respect to label efficiency (since our method mainly relies on large amounts of unlabeled data, which are inexpensive to gather).

However, our work still has certain limitations. As can also be seen in Appendix D.5, our method requires some prior knowledge of the type of distortions that will be applied to the image. This is due to the fact that our method relies on training the student to match the representations of the teacher, which is significantly more difficult when the type of noise (and thus, the representation itself) changes drastically. As future work, we aim to extend our method beyond this limitation, possibly by finetuning the teacher as well as the student, to produce representations that are more easily matched under different types of noise. Moreover, due to hardware constraints we had to use only a part of the ImageNet dataset for training, and only a relatively small batch size, which is an important consideration for contrastive learning [6]. However, even if we may have obtained better results with more data and a larger batch size, this is not detrimental to the overall impact of our work, since training an equally powerful model from scratch is far more expensive in both aspects.

Acknowledgements

This research has been supported by NSF Grants CCF 1763702,1934932, AF 1901292, 2008710, 2019844 research gifts by Western Digital, WNCG IAP, computing resources from TACC and the Archie Straiton Fellowship.

References

- [1] M. Asim, A. Ahmed, and P. Hand. Invertible generative models for inverse problems: mitigating representation error and dataset bias. *arXiv preprint arXiv:1905.11672*, 2019.
- [2] A. Buades, B. Coll, and J.-M. Morel. Non-local means denoising. *Image Processing On Line*, 1:208–212, 2011.
- [3] C. Bucila, R. Caruana, and A. Niculescu-Mizil. Model compression. In *KDD '06*, 2006.
- [4] M. Caron, I. Misra, J. Mairal, P. Goyal, P. Bojanowski, and A. Joulin. Unsupervised learning of visual features by contrasting cluster assignments. *arXiv preprint arXiv:2006.09882*, 2020.
- [5] T. Chen and L. Li. Intriguing properties of contrastive losses. *CoRR*, abs/2011.02803, 2020. URL <https://arxiv.org/abs/2011.02803>.

- [6] T. Chen, S. Kornblith, M. Norouzi, and G. E. Hinton. A simple framework for contrastive learning of visual representations. *ArXiv*, abs/2002.05709, 2020.
- [7] T. Chen, S. Kornblith, K. Swersky, M. Norouzi, and G. E. Hinton. Big self-supervised models are strong semi-supervised learners. *ArXiv*, abs/2006.10029, 2020.
- [8] A. Coates, A. Ng, and H. Lee. An analysis of single-layer networks in unsupervised feature learning. In G. Gordon, D. Dunson, and M. Dudík, editors, *Proceedings of the Fourteenth International Conference on Artificial Intelligence and Statistics*, volume 15 of *Proceedings of Machine Learning Research*, pages 215–223, Fort Lauderdale, FL, USA, 11–13 Apr 2011. PMLR. URL <http://proceedings.mlr.press/v15/coates11a.html>.
- [9] J. P. Cohen, P. Morrison, and L. Dao. Covid-19 image data collection. *arXiv 2003.11597*, 2020. URL <https://github.com/ieee8023/covid-chestxray-dataset>.
- [10] M. Z. Darestani, A. Chaudhari, and R. Heckel. Measuring robustness in deep learning based compressive sensing. *arXiv preprint arXiv:2102.06103*, 2021.
- [11] M. Dhar, A. Grover, and S. Ermon. Modeling sparse deviations for compressed sensing using generative models. *arXiv preprint arXiv:1807.01442*, 2018.
- [12] S. Dodge and L. Karam. A study and comparison of human and deep learning recognition performance under visual distortions. In *2017 26th International Conference on Computer Communication and Networks (ICCCN)*, pages 1–7, 2017. doi: 10.1109/ICCCN.2017.8038465.
- [13] F. L. Gómez, A. Eftekhari, and V. Cevher. Fast and provable admm for learning with generative priors. *arXiv preprint arXiv:1907.03343*, 2019.
- [14] M. Gutmann and A. Hyvärinen. Noise-contrastive estimation: A new estimation principle for unnormalized statistical models. In Y. W. Teh and M. Titterton, editors, *Proceedings of the Thirteenth International Conference on Artificial Intelligence and Statistics*, volume 9 of *Proceedings of Machine Learning Research*, pages 297–304, Chia Laguna Resort, Sardinia, Italy, 13–15 May 2010. PMLR. URL <http://proceedings.mlr.press/v9/gutmann10a.html>.
- [15] K. He, H. Fan, Y. Wu, S. Xie, and R. Girshick. Momentum contrast for unsupervised visual representation learning. In *Proceedings of the IEEE/CVF Conference on Computer Vision and Pattern Recognition (CVPR)*, June 2020.
- [16] R. Heckel and P. Hand. Deep decoder: Concise image representations from untrained non-convolutional networks. *arXiv preprint arXiv:1810.03982*, 2018.
- [17] O. Henaff. Data-efficient image recognition with contrastive predictive coding. In H. D. III and A. Singh, editors, *Proceedings of the 37th International Conference on Machine Learning*, volume 119 of *Proceedings of Machine Learning Research*, pages 4182–4192. PMLR, 13–18 Jul 2020. URL <http://proceedings.mlr.press/v119/henaff20a.html>.
- [18] D. Hendrycks and T. Dietterich. Benchmarking neural network robustness to common corruptions and perturbations. In *International Conference on Learning Representations*, 2019. URL <https://openreview.net/forum?id=HJz6tiCqYm>.
- [19] G. Hinton, O. Vinyals, and J. Dean. Distilling the knowledge in a neural network. In *NIPS Deep Learning and Representation Learning Workshop*, 2015. URL <http://arxiv.org/abs/1503.02531>.
- [20] C.-H. Ho and N. Vasconcelos. Contrastive learning with adversarial examples. Oct. 2020.
- [21] H. Hosseini, B. Xiao, and R. Poovendran. Google’s cloud vision api is not robust to noise. *2017 16th IEEE International Conference on Machine Learning and Applications (ICMLA)*, pages 101–105, 2017.
- [22] Z. Jiang, T. Chen, T. Chen, and Z. Wang. Robust pre-training by adversarial contrastive learning. In *NeurIPS*, 2020.
- [23] M. Kabkab, P. Samangouei, and R. Chellappa. Task-aware compressed sensing with generative adversarial networks. In *Thirty-Second AAAI Conference on Artificial Intelligence*, 2018.
- [24] P. Khosla, P. Teterwak, C. Wang, A. Sarna, Y. Tian, P. Isola, A. Maschinot, C. Liu, and D. Krishnan. Supervised contrastive learning. Apr. 2020.
- [25] M. Kim, J. Tack, and S. J. Hwang. Adversarial Self-Supervised contrastive learning. June 2020.
- [26] D. P. Kingma and J. Ba. Adam: A method for stochastic optimization. *CoRR*, abs/1412.6980, 2015.

- [27] K. Kotar, G. Ilharco, L. Schmidt, K. Ehsani, and R. Mottaghi. Contrasting contrastive Self-Supervised representation learning models. Mar. 2021.
- [28] A. Krizhevsky. Learning multiple layers of features from tiny images. 2009.
- [29] D. Lee. Pseudo-label : The simple and efficient semi-supervised learning method for deep neural networks. 2013.
- [30] M. Lustig, D. Donoho, and J. M. Pauly. Sparse mri: The application of compressed sensing for rapid mr imaging. *Magnetic Resonance in Medicine: An Official Journal of the International Society for Magnetic Resonance in Medicine*, 58(6):1182–1195, 2007.
- [31] G. Ongie, A. Jalal, C. A. Metzler, R. G. Baraniuk, A. G. Dimakis, and R. Willett. Deep learning techniques for inverse problems in imaging. *IEEE Journal on Selected Areas in Information Theory*, 1(1):39–56, 2020.
- [32] A. Oord, Y. Li, and O. Vinyals. Representation learning with contrastive predictive coding. *ArXiv*, abs/1807.03748, 2018.
- [33] P. Pandit, M. Sahraee-Ardakan, S. Rangan, P. Schniter, and A. K. Fletcher. Inference with deep generative priors in high dimensions. *arXiv preprint arXiv:1911.03409*, 2019.
- [34] A. Paszke, S. Gross, F. Massa, A. Lerer, J. Bradbury, G. Chanan, T. Killeen, Z. Lin, N. Gimelshein, L. Antiga, A. Desmaison, A. Kopf, E. Yang, Z. DeVito, M. Raison, A. Tejani, S. Chilamkurthy, B. Steiner, L. Fang, J. Bai, and S. Chintala. Pytorch: An imperative style, high-performance deep learning library. In H. Wallach, H. Larochelle, A. Beygelzimer, F. d'Alché-Buc, E. Fox, and R. Garnett, editors, *Advances in Neural Information Processing Systems 32*, pages 8024–8035. Curran Associates, Inc., 2019. URL <http://papers.neurips.cc/paper/9015-pytorch-an-imperative-style-high-performance-deep-learning-library.pdf>.
- [35] A. Radford, J. W. Kim, C. Hallacy, A. Ramesh, G. Goh, S. Agarwal, G. Sastry, A. Askell, P. Mishkin, J. Clark, G. Krüger, and I. Sutskever. Learning transferable visual models from natural language supervision. <https://openai.com/blog/clip/>, 2021.
- [36] O. Russakovsky, J. Deng, H. Su, J. Krause, S. Satheesh, S. Ma, Z. Huang, A. Karpathy, A. Khosla, M. S. Bernstein, A. Berg, and L. Fei-Fei. Imagenet large scale visual recognition challenge. *International Journal of Computer Vision*, 115:211–252, 2015.
- [37] J. Scarlett and V. Cevher. Limits on support recovery with probabilistic models: An information-theoretic framework. *IEEE Transactions on Information Theory*, 63(1):593–620, 2016.
- [38] D. Temel, J. Lee, and G. Alregib. Cure-or: Challenging unreal and real environments for object recognition. In *2018 17th IEEE International Conference on Machine Learning and Applications (ICMLA)*, pages 137–144, 2018. doi: 10.1109/ICMLA.2018.00028.
- [39] Y. Tian, D. Krishnan, and P. Isola. Contrastive multiview coding. *arXiv preprint arXiv:1906.05849*, 2019.
- [40] Y. Tian, D. Krishnan, and P. Isola. Contrastive representation distillation. In *International Conference on Learning Representations*, 2020. URL <https://openreview.net/forum?id=SkgpBJrtvS>.
- [41] Y. Tian, L. Yu, X. Chen, and S. Ganguli. Understanding self-supervised learning with dual deep networks. *CoRR*, abs/2010.00578, 2020. URL <https://arxiv.org/abs/2010.00578>.
- [42] T. Wang and P. Isola. Understanding contrastive representation learning through alignment and uniformity on the hypersphere. In *ICML*, 2020.
- [43] Z. Wu, Y. Xiong, S. X. Yu, and D. Lin. Unsupervised feature learning via non-parametric instance discrimination. In *Proceedings of the IEEE Conference on Computer Vision and Pattern Recognition (CVPR)*, June 2018.
- [44] Q. Xie, E. Hovy, M.-T. Luong, and Q. V. Le. Self-training with noisy student improves imagenet classification. *2020 IEEE/CVF Conference on Computer Vision and Pattern Recognition (CVPR)*, pages 10684–10695, 2020.
- [45] Y. Zhou, S. Song, and N.-M. Cheung. On classification of distorted images with deep convolutional neural networks. In *2017 IEEE International Conference on Acoustics, Speech and Signal Processing (ICASSP)*, pages 1213–1217, 2017. doi: 10.1109/ICASSP.2017.7952349.

Appendix

A Broader Impact

As previously mentioned, the goal of our work is to create an image classification system which is robust to various distortions on the input data, which has potential applications on improving the practical use of neural network architectures. However, we have to point out some ethical considerations for the use of our work. On the one hand, allowing more applications to access the power of deep learning may not necessarily have a positive impact, since this largely depends on the goals of the application itself. On the other hand, care should be taken when choosing the dataset on which to train the student encoder, as well as the model to serve as the teacher encoder. Since our proposed process aims to distill information from the teacher, as well as use a specific dataset to perform classification, the presence of biases in either may carry over to our student encoder, which is undesirable. It is paramount for the ethical application of our work to distill information from models without any such biases.

B Proof of Proposition 1

Proposition 2. *If R is a minimizer of the uniformity term*

$$R \in \arg \min_f \sum_{i=1}^N \log \sum_{j=1}^N \exp \frac{\langle f(x_i), f(x_j) \rangle}{\tau},$$

then any encoder $S^ \in \arg \min_S \hat{\mathcal{L}}^{\text{contr}}(S; \tau, R, A)$ exactly recovers the target embedding, $S^*(A(x_i)) = R(x_i)$ for all x_i in the training set.*

Proof. We are interested in the minimizers of the function $\hat{\mathcal{L}}^{\text{contr}}$. To simplify notation, we denote $R(x_i)$ as R_i , $S(A(x_i))$ as S_i and

$$H_R(x) := \sum_j \exp \langle x, R_j \rangle / \tau.$$

We also denote

$$F_i(S_i) := -\langle S_i, R_i \rangle + \tau \log H_R(S_i)$$

such that

$$\hat{\mathcal{L}}^{\text{contr}}(S; \tau, R, A) = \frac{1}{\tau \cdot N} \sum_{j=1}^N F_i(S_i).$$

Since each S_i only appears in one term of the above sum, it suffices to show that F_i is uniquely minimized by the argument R_i . The only assumption we make on R_i follows from [42] which shows that if R minimizes the uniformity term, then $\sum_j R_j = 0$.

We prove the claim directly by showing that $F_i(S_i) - F_i(R_i) > 0$ for any S_i with $\|S_i\| = 1$ and $S_i \neq R_i$. Fix some S_i with norm 1 and suppose that $\langle S_i, R_i \rangle = 1 - \delta$. Then from an argument by cosine distance, we see that replacing R_i with S_i cannot alter the dot product $\langle R_i, R_j \rangle$ by more than δ for any j : $|\langle R_i - S_i, R_j \rangle| \leq \delta$ for all R_j . Using optimality of R , we claim there exists some j such that this is strict on one side. There must exist a j such that

$$\langle R_j, S_i \rangle > \langle R_j, R_i \rangle - \delta,$$

because if not, then $\langle R_j, S_i \rangle = \langle R_j, R_i \rangle - \delta$ for all j . Summing both sides over j and using the fact that $\sum_j R_j = 0$ generates the contradiction that $0 = -N\delta$.

Now we decompose the $H_R(S_i)$ term inside $F_i(S_i)$:

$$\begin{aligned} H_R(S_i) &= \sum_j \exp(\langle S_i, R_j \rangle / \tau) \\ &> e^{-\delta/\tau} \cdot \sum_j \exp(\langle R_i, R_j \rangle / \tau) \\ &= e^{-\delta/\tau} \cdot H_R(R_i), \end{aligned}$$

where the inequality follows from $\exp(\langle S_i, R_j \rangle / \tau) \geq \exp(\langle R_i, R_j \rangle / \tau - \delta / \tau)$ for all j , where it is strict for at least one j . We can now directly compare $F_i(S_i)$ to $F_i(R_i)$ as

$$\begin{aligned} F_i(x) - F_i(R_i) &= \langle R_i, R_i - S_i \rangle + \tau \cdot (\log H_R(S_i) - \log H_R(R_i)) \\ &= \delta + \tau \cdot (\log H_R(S_i) - \log H_R(R_i)) \\ &> \delta + \tau \cdot \log e^{-\delta/\tau} = 0. \end{aligned}$$

Hence, f_i has a unique global minimizer at R_i . \square

C Variants on the Uniformity Term

As mentioned in the main text, in Section 3, we consider variations on the uniformity term in $\hat{\mathcal{L}}^{\text{contr}}$. We explicitly define these variations here. Recall that

$$\hat{\mathcal{L}}^{\text{contr}}(S; \tau, R, A) := \frac{1}{\tau} \hat{\mathcal{L}}^{\text{MSE}}(S; R, A) + \hat{\mathcal{L}}^{\text{unif}}(S; \tau, R, A).$$

In the main text, we use the ‘student vs. teacher’ uniformity loss. We explicitly define this variant and all others considered in the following list. We abuse notation slightly and use the function $K_\tau(\cdot, \cdot)$ defined as:

$$K_\tau(y, z) := \exp(\langle y, z \rangle / \tau),$$

noting that in the main text the arguments to K were *indices* and here they the *embedding vectors* themselves. As above, we let $S(A(x_i))$ and $R(x_i)$ be denoted by S_i, R_i respectively.

- **Student vs. Teacher:** This loss compares the noisy student embeddings to the clean teacher embeddings, denoted as

$$\hat{\mathcal{L}}_{ST}^{\text{unif}}(S; \tau, R, A) := \frac{1}{N} \sum_i \log \sum_j K_\tau(S_i, R_j)$$

- **Student vs. Student:** This loss compares pairs of noisy student embeddings:

$$\hat{\mathcal{L}}_{ST}^{\text{unif}}(S; \tau, R, A) := \frac{1}{N} \sum_i \log \sum_{j \neq i} K_\tau(S_i, S_j)$$

- **Student vs. Both:** This loss combines the above two losses, where the combination occurs *inside the logarithm*:

$$\hat{\mathcal{L}}_{SB}^{\text{unif}}(S; \tau, R, A) := \frac{1}{N} \sum_i \log \left(\sum_{j \neq i} K_\tau(S_i, S_j) + \sum_j K_\tau(S_i, R_j) \right)$$

- **NT-XEnt:** This loss includes terms for the pairwise similarity between all $4N^2 - 2N$ pairs of student and teacher embeddings. We denote this as *NT - XEnt*, because in the contrastive setting where data is provided in terms of batches of paired positive examples $\{x_i, x_i^+\}$, all pairs are considered in the contrastive loss.

$$\begin{aligned} \hat{\mathcal{L}}_{NT}^{\text{unif}}(S; \tau, R, A) &:= \frac{1}{N} \sum_i \left(\log \left(\sum_{j \neq i} K_\tau(S_i, S_j) + \sum_j K_\tau(S_i, R_j) \right) + \right. \\ &\quad \left. \log \left(\sum_j K_\tau(R_i, S_j) + \sum_{j \neq i} K_\tau(R_i, R_j) \right) \right). \end{aligned}$$

D Further Experiments and Experimental Details

D.1 Training Details

Datasets For all experiments, we pre-train the robust encoder as well as the baseline using a randomly chosen 100-class subset of the ImageNet dataset [36]. ImageNet consists of 1,000 classes

of objects, with 1.2M training images and 50K validation images. The portion we use is the same subset of ImageNet used by [39], and contains 126,689 training and 5,000 validation images. We refer to this dataset as ImageNet-100.

For the transfer learning task, we make use of five datasets: (1) CIFAR-10 [28], (2) CIFAR-100 [28], and (3) STL-10 [8]. (4) The COVID-19 Chest X-ray dataset [9], which consists of X-rays taken of patients with healthy lungs as well as lungs affected by pneumonia resulting from COVID-19. The dataset contains 5,286 training images and 624 test images. (5) We generate another random 100-class subset of ImageNet [36] from the remaining 900 classes we did not use for ImageNet-100, which we refer to as ImageNet-100B. This subset contains 128,987 training images and 5,000 validation images.

Image Pre-Processing During contrastive training, we randomly crop the image and resize it to a height and width of 224 pixels, then apply a random horizontal flip. The resultant image is normalized to have a mean of 0 and standard deviation 1 in each color channel before being fed to the input of the teacher. A copy of the randomly-cropped and flipped image is distorted with a given forward operator and normalized to feed to the student input. We pre-process the images for training the baseline by applying a random crop, resizing to 224×224 pixels, applying a given distortion, and normalizing the pixel values. During validation and testing, we resize each image to a height and width of 256 pixels, take a center crop of 224×224 pixels, apply a distortion, and finally normalize the image. We vary the train and test distortions depending on the setting we evaluate.

For images from CIFAR-10, CIFAR-100, and STL-10, we pre-process the training images by resizing to 224×224 pixels, applying a random horizontal flip, distorting with a given forward operator, and finally normalizing the images. For validation images from these datasets we perform the same process without the random flip. For training images from the COVID-19 X-ray dataset and ImageNet-100B, we apply a random crop, resize to 224×224 pixels, apply a given distortion, and normalize the pixel values. For validation images from these datasets, instead of a random crop and resize, we resize to 256×256 pixels and take a 224×224 center crop of the image, then apply a distortion and normalize.

We apply random pixel masking, Gaussian blur, and additive Gaussian noise as our distortions in the various settings we evaluate. Random pixel masking sets the intensity of a randomly-chosen set of pixels in an image to 0. Gaussian blur convolves the image with an isotropic Gaussian kernel, and additive Gaussian noise applies additive white gaussian noise to each each pixel in the image.

Training Hyperparameters We train our method and the supervised baseline using the Adam optimizer with default values for β and a cosine learning rate schedule [26]. For the baseline, we use a learning rate of 0.001 and a batch size of 64. For our method, we use a learning rate of 0.0003, weight decay of 0.0001 and a batch size of 256, and we set the temperature τ from Eq (3) to be 0.1. We train both the baseline and our method for 25 epochs. The baseline is optimized using cross entropy loss.

We train a linear classifier on top of the learned representations for our method and the baseline for each set of experiments. The linear classification layer is optimized with the Adam optimizer, using a learning rate of 0.001 and a batch size of 128, and is trained for 10 epochs. For label-efficiency experiments, we lower the batch size to 8 to compensate for the decrease in the data used. We freeze the learned backbone network during training of the classifier. The classifier is trained using images that have the same distortions as were used to train the backbone network. During transfer learning using the baseline, we remove the classification layer used on ImageNet-100 pre-training and replace it with a randomly-initialized layer with appropriate dimension.

We choose the hyperparameters for each model using a linear search over several values for each hyperparameter, based on the highest mean validation accuracy we achieve on ImageNet-100 after one epoch of training on each distortion type.

All experiments were performed on a system with 4 Nvidia Quadro RTX5000 GPUs, 2 Intel Xeon E5-2620 v4 CPUs, and 128GB of RAM. Experiments using CLIP networks were run using 16-bit floating point models and data. We use the PyTorch implementation of the supervised ImageNet-trained ResNet-101 [34].

D.2 Top-5 Results for Main Experiments

For sake of completeness, we provide the full metrics for our experiments, which also include top-5 accuracies for the experiments performed. The conclusions we can draw from the top-1 accuracy results do not change when we look at the top-5 accuracies.

For the transfer learning task on COVID X-ray data, we present the area under the receiver operating characteristic curve (AUC). This dataset presents a binary classification problem, so top-5 metrics do not apply.

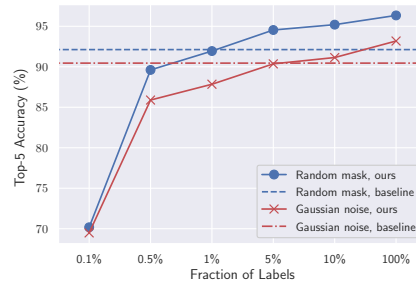


Figure 7: **Top-5 accuracies using a varying fraction of labeled samples to train a linear probe.** We train robust encoders on images with 90% random pixel masking and additive Gaussian noise with standard deviation 0.5, and fit a linear classifier on the learned representations using varying fractions of labeled training samples. We compare to a supervised baseline that uses all of the labeled training samples. Results are averaged over 10 random instantiations of corruptions on the ImageNet-100 validation dataset. We omit error bars as standard error is insignificant.

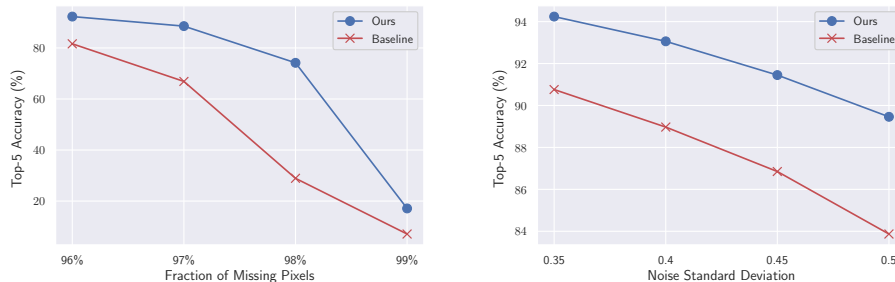


Figure 8: **Top-5 accuracies for images with varying corruption levels using models trained on a range of levels.** In the left figure, we compare our robust model with a baseline, both trained on images with 50% to 95% random pixel masking. In the right figure, each model is trained on images with additive Gaussian noise with random standard deviation from 0.1 to 0.3. We evaluate the models on images with more severe corruptions than applied during training. Results are averaged over 10 random instantiations of corruptions on the ImageNet-100 validation dataset. We omit error bars as standard error is insignificant.

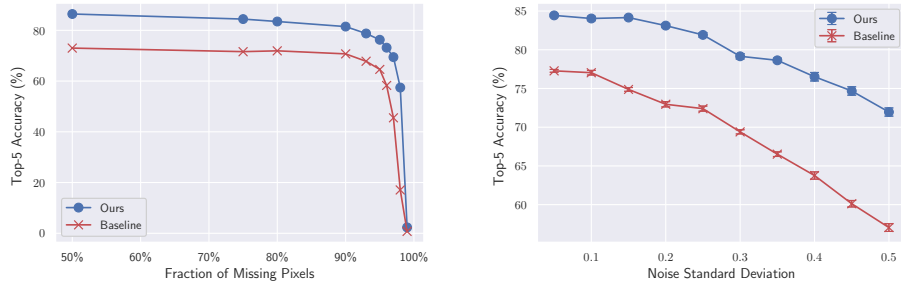


Figure 9: **Top-5 accuracies for varying noise levels on unseen classes using label shift.** On the left, we see the model trained on 50% to 95% random masking of pixels, while on the right the model trained on Gaussian noise with standard deviation from 0.1 to 0.3. Both models are evaluated on the unseen classes, using the chosen reference classes from ImageNet100 as the targets, as shown in the label shift table. Results are averaged over 10 random instantiations of corruptions. We omit error bars in the left figure as standard error is insignificant.

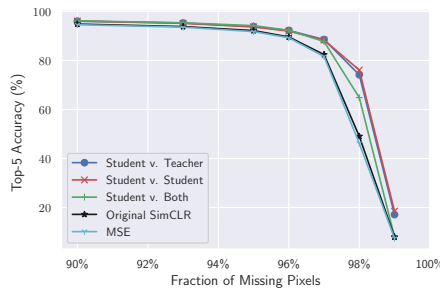


Figure 10: **Ablation study with top-5 accuracies.** We evaluate the model trained on 50% to 95% random masking of pixels, using several variants of the uniformity term in the contrastive loss. Results are averaged over 10 random instantiations of corruptions on the ImageNet-100 validation dataset. We omit error bars as standard error is insignificant.

Table 4: **Top-5 accuracy (percent) on ImageNet-100.** The best accuracy for each distortion is bolded. Each model is trained using images with a fixed type of distortion. We train our robust CLIP encoder contrastively, then fit a linear probe on the learned representations using either all or 10% of the labeled training samples. We report the mean and standard error for accuracy over 10 random instantiations of distortions on the ImageNet-100 validation dataset (Gaussian blur is deterministic, so we do not include standard error values). For Gaussian blur, n corresponds to the length of the blur kernel.

Distortion	Supervised Baseline	Ours	Ours (10% labeled data)
Random Mask 50%	93.86±0.04	97.60±0.02	96.57±0.06
Random Mask 75%	93.19±0.05	96.83±0.06	95.53±0.05
Random Mask 90%	92.12±0.05	96.34±0.04	95.20±0.04
Gaussian Noise $\sigma = 0.1$	95.49±0.03	97.39±0.04	96.11±0.03
Gaussian Noise $\sigma = 0.3$	93.00±0.05	95.59±0.07	93.95±0.06
Gaussian Noise $\sigma = 0.5$	90.45±0.05	93.18±0.06	91.14±0.06
Gaussian Blur $n = 21$	93.38	96.34	95.26
Gaussian Blur $n = 37$	89.42	93.94	91.88

Table 5: **Top-5 accuracies for transfer learning.** We fit a linear classifier for each dataset on top of the representations learned by the models from ImageNet-100. RM means the model was trained with random missing pixels, and GN means it was trained with additive Gaussian noise. Results are mean and standard errors over 10 realizations of the distortions during evaluation. The COVID X-ray dataset has two classes so there are no top-5 results.

Model	CIFAR-10	CIFAR-100	STL-10	ImageNet-100B
Baseline (RM)	98.92±0.02	84.09±0.05	99.38±0.01	88.35±0.04
Ours (RM)	99.23±0.02	86.26±0.04	99.72±0.01	95.40±0.04
Baseline (GN)	98.76±0.02	81.37±0.05	99.41±0.01	89.81±0.08
Ours (GN)	98.72±0.02	81.50±0.06	99.48±0.01	94.74±0.06

Table 6: **Area under receiver operating characteristic curve (AUC) for transfer learning on COVID X-ray data.** We fit a linear classifier for the COVID X-ray dataset on top of the representations learned by the models from ImageNet-100. RM means the model was trained with random missing pixels, and GN means it was trained with additive Gaussian noise. Results are mean and standard errors over 10 realizations of the distortions during evaluation.

Model	AUC
Baseline (RM)	0.918±0.0011
Ours (RM)	0.918±0.0010
Baseline (GN)	0.927±0.0009
Ours (GN)	0.896±0.0015

D.3 Comparisons with Denoising and Inpainting for Classification

An alternative way of solving the inverse problem presented in the paper is to use methods which operate directly on the pixel space of the image. Instead of training a classifier which operates on distorted images, one could try to recover the original images from the distorted version. The recovered images can then be given to a classifier trained on clean images. We compare our method with two such baselines which operate in pixel space:

1. We apply Non-Local Means (NLM) [2] denoising to images corrupted by additive Gaussian noise.
2. We use Deep Decoder [16] with default parameters and 5000 optimization steps to perform inpainting on images with random missing pixels. Deep Decoder is a method which randomly initializes an under-parameterized generative network with upsampling and 1×1 convolution layers, then optimizes over the weights of the network to fit a single distorted image. Since the network is underparameterized, it cannot fit noise very well, while its upsampling and convolution layers bias it to produce natural-looking images. The result is that the network produces a reconstructed version of the original image, despite never having been trained on any other data.

For evaluation, we corrupt images from the ImageNet-100 validation set with Gaussian noise and random pixel masks, then apply NLM and Deep Decoder, respectively. We feed the recovered images as input to a classification model trained on clean image data. The classification model we use is an ImageNet pre-trained ResNet-101 backbone with a linear classifier trained on clean ImageNet-100 images. We compare the performance of these pixel-space inverse methods with that of our method. The results for denoising are seen in Table 7 and the results for inpainting in Table 8. We can see that the inverse methods acting in pixel space are not reliable at reconstructing images for classification. In the case of denoising the accuracy degrades quickly with increasing noise, and for inpainting the accuracy is poor for all masking levels.

Table 7: **Denoising baseline.** We compare our method to a 2-step denoising baseline, where a) we denoise images with various levels of additive Gaussian noise using Non-Local Means denoising and b) we feed the images through a model trained on clean images from ImageNet-100. Results for our method are included for comparison. We perform 10 evaluation runs for each experiment and present the mean and standard error.

Noise Level	Denoising	Ours
$\sigma = 0.1$	73.49±0.08	84.46±0.08
$\sigma = 0.3$	56.47±0.14	81.30±0.07
$\sigma = 0.5$	27.64±0.14	76.23±0.10

Table 8: **Inpainting baseline.** We compare our method to an inpainting baseline, where a) we inpaint images with varying fractions of missing pixels using Deep Decoder [16] and b) we feed the images through a model trained on clean images from ImageNet-100. Results from the main paper are included for comparison.

Missing Pixel Fraction	Inpainting	Ours
50%	23.38	85.87
75%	21.89	83.99
90%	20.39	82.96

D.4 Transferring a Clean Classifier to Robust Encoders

To demonstrate the ability of our method to retrieve good representations from the teacher, we perform the following experiment. We train a robust encoder on distorted images using the method we propose. We then train a linear classifier on top of the pre-trained, non-robust CLIP backbone using clean images. Finally, we transfer this linear classifier for clean images to the robust encoder. The results can be seen in Table 9. We see that our technique achieves good results, even without finetuning the linear classifier on distorted images. This means that the representations learned by the student for distorted images are sufficiently close to those of the teacher for clean images.

Table 9: **Accuracies for applying a linear classifier trained on clean images on top of representations from a robust CLIP encoder.** We transfer the linear classifier trained on clean images on top of the representations learned by our contrastive technique. We evaluate on the same noises used during training of the robust encoder. Best scores are not bolded since we intend to illustrate a quality of our method instead of comparing two techniques.

Distortion	Clean Linear Classifier	Ours
Random Mask 50%	80.1	85.87
Random Mask 75%	76.4	83.99
Random Mask 90%	78.1	82.96
Gaussian Noise $\sigma = 0.1$	77.2	84.46
Gaussian Noise $\sigma = 0.3$	75.7	81.30
Gaussian Noise $\sigma = 0.5$	70.5	76.23
Gaussian Blur $n = 21$	78.3	83.24
Gaussian Blur $n = 37$	73.1	77.80

D.5 Experiments on ImageNet-100C

As a final benchmark, we compare our methods on a subset of ImageNet-C [18] with the same classes as those of ImageNet-100, henceforth referred to as ImageNet-100C. We compare two models:

- The first is a baseline ResNet-101, pretrained on ImageNet and finetuned on clean images of ImageNet-100.
- The second is a version of our student encoder, which is initialized from CLIP and is trained on distorted images. On these images, Gaussian blurring with $\sigma \in [1, 5]$ and Gaussian additive noise with $\sigma \in [0.05, 0.5]$ are applied, independently with probability 0.8 each.

Results can be seen in Table 10. The values for the methods on each corruption type are top-1 accuracies averaged across 5 levels of corruption. We can see here that our model does not get results comparable to the baseline. This can be explained by a limitation of our current work, in that we rely on student representations matching the teacher representations. If the *type* of noise is altered for the student, then it is difficult for it to match the teacher representations, which are fixed. Indeed, altering the type of noise on an image is expected to greatly affect its representation. Thus, at its present iteration, our technique relies on some prior knowledge about the *type* of distortion encountered. Possible ways around this, such as also finetuning the teacher, are left for consideration in future work.

Table 10: **ImageNet-100C results.** We present the mean top-1 accuracies across 5 corruption levels for each corruption type. We do not present mean corruption error (mCE) as this is computed with respect to performance on full ImageNet-C, while we compute on a 100-class subset of ImageNet-C.

	Corruption	Supervised Baseline	Ours
Blur	Defocus	61.76	56.88
	Glass	49.15	50.52
	Motion	59.38	44.37
	Zoom	59.00	50.69
Digital	Contrast	58.61	43.69
	Elastic	67.85	60.40
	JPEG	77.75	61.08
	Pixelate	73.06	75.65
Noise	Gaussian	55.83	56.81
	Impulse	51.05	54.11
	Shot	53.76	56.74
Weather	Brightness	86.01	72.57
	Fog	67.56	54.20
	Frost	59.58	51.70
	Snow	53.97	39.80
Extra	Gaussian Blur	64.31	62.66
	Saturate	82.16	65.95
	Spatter	71.9	59.52
	Speckle	62.65	66.28

D.6 ImageNet-100 Classes

To train our model and the baseline, we use a randomly-chosen 100-class subset of the original ImageNet dataset. This subset is the same as used in [39]. We present the `wnid` of each of the classes in the subset in Table 11

D.7 ImageNet-100B Classes

For the transfer learning experiments, we select a random subset of 100 classes from ImageNet which are mutually exclusive with the classes found in ImageNet-100. We term this subset ImageNet-100B, and present the `wnid` of each of the classes used in this subset in Table 12.

Table 11: **List of ImageNet-100 Classes.** We present the `wnid` of each of the classes used in ImageNet-100. These classes are randomly sampled from the original ImageNet dataset and are the same classes used in [39].

ImageNet-100 Classes				
n02869837	n02086910	n03785016	n02483362	n03837869
n01749939	n02859443	n03764736	n04127249	n03494278
n02488291	n13040303	n03775546	n02089973	n04136333
n02107142	n03594734	n02087046	n03017168	n03794056
n13037406	n02085620	n07836838	n02093428	n03492542
n02091831	n02099849	n04099969	n02804414	n02018207
n04517823	n01558993	n04592741	n02396427	n04067472
n04589890	n04493381	n03891251	n04418357	n03930630
n03062245	n02109047	n02701002	n02172182	n03584829
n01773797	n04111531	n03379051	n01729322	n02123045
n01735189	n02877765	n02259212	n02113978	n04229816
n07831146	n04429376	n07715103	n03787032	n02100583
n07753275	n02009229	n03947888	n02089867	n03642806
n03085013	n01978455	n04026417	n02119022	n04336792
n04485082	n02106550	n02326432	n03777754	n03259280
n02105505	n01820546	n03637318	n04238763	n02116738
n01983481	n01692333	n01980166	n02231487	n02108089
n02788148	n07714571	n02113799	n03032252	n03424325
n03530642	n02974003	n02086240	n02138441	n01855672
n04435653	n02114855	n03903868	n02104029	n02090622

Table 12: **List of ImageNet-100B Classes.** We present the `wnid` of each of the classes used in ImageNet-100B. These classes are randomly sampled from the original ImageNet dataset and are mutually exclusive with the classes in ImageNet-100.

ImageNet-100B Classes				
n02088364	n02840245	n04258138	n03670208	n02013706
n03000134	n01688243	n02280649	n03483316	n02797295
n03544143	n03920288	n02492660	n02777292	n04366367
n03388043	n02488702	n03782006	n03602883	n03857828
n02165105	n03884397	n03495258	n03982430	n04243546
n02321529	n07745940	n04254120	n02808440	n03891332
n01819313	n01484850	n02391049	n03207743	n03796401
n03187595	n04147183	n04254777	n02096177	n03314780
n01667114	n04356056	n07716906	n01742172	n04039381
n02097130	n01644900	n03888605	n03792782	n01498041
n02104365	n02132136	n01843065	n01795545	n01990800
n02279972	n02999410	n02643566	n03534580	n03976657
n12985857	n02457408	n04515003	n03814906	n02107683
n01773549	n04540053	n03125729	n02342885	n02229544
n12057211	n02776631	n04179913	n03692522	n03063599
n02791270	n02107574	n03788365	n03272010	n03127747
n01491361	n02930766	n02098286	n09468604	n03179701
n02169497	n04263257	n02109525	n03720891	n03016953
n02793495	n03724870	n02966193	n03717622	n09193705
n02281787	n04081281	n03929660	n02177972	n04033901

E Visualization of Distortions

In this section, we present several examples of the fixed distortions we apply during training and testing. All images are taken from the ImageNet-100 validation set.

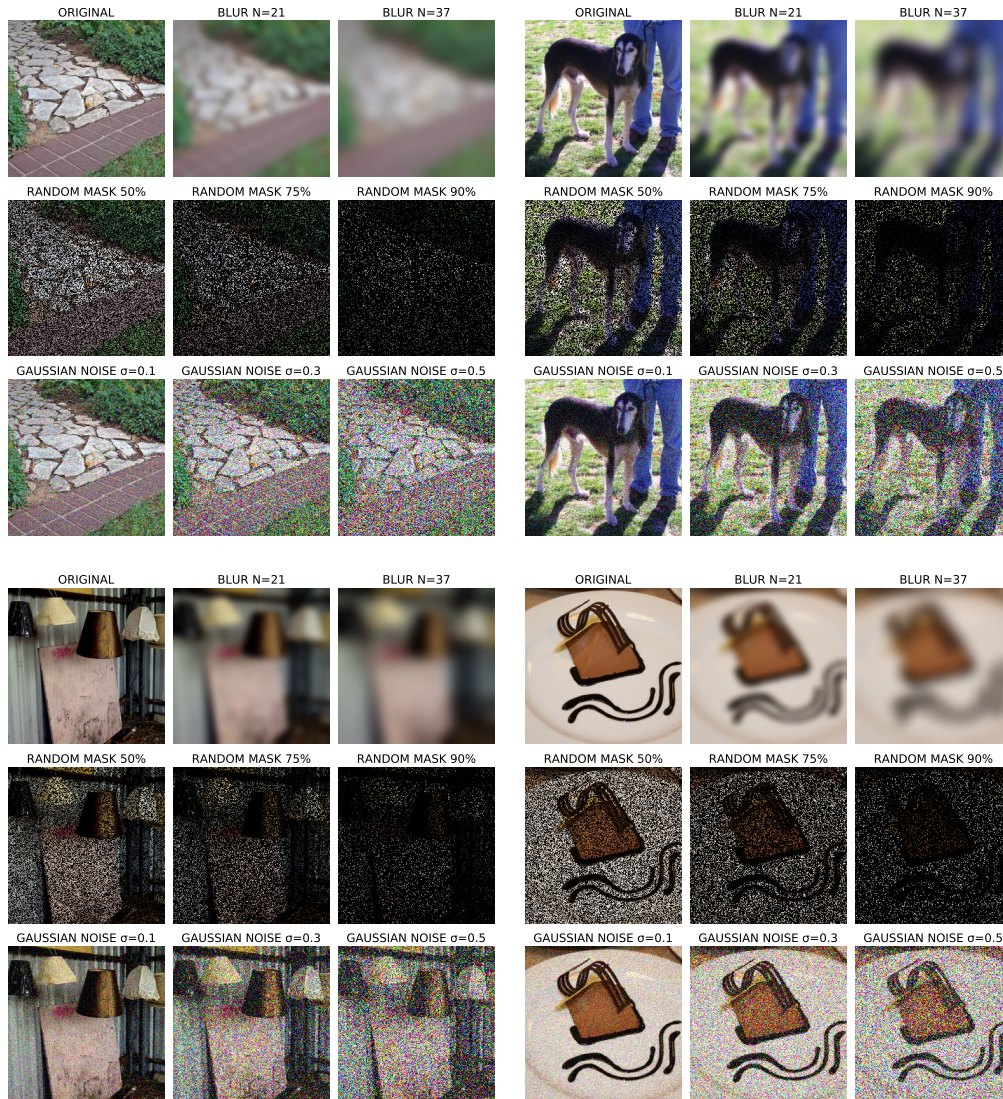


Figure 11: Visualization of the various fixed distortions we test.